Towards realistic DEM modeling of blast furnace mixture charging

Calibration and verification of model parameters under high-velocity flow conditions

Roeplal, Raïsa; Pang, Yusong; Schott, Dingena

DOI
10.1016/j.powtec.2025.121382

Publication date
2026

Document Version
Final published version

Published in
Powder Technology

Powder Technology 467 (2026) 121382

Contents lists available at ScienceDirect

Powder Technology

journal homepage: www.journals.elsevier.com/powder-technology

Towards realistic DEM modeling of blast furnace mixture charging: Calibration and verification of model parameters under high-velocity flow conditions

Raïsa Roeplal *, Yusong Pang, Dingena Schott

Department of Maritime and Transportation Technology, Faculty of Mechanical Engineering, TU Delft, Mekelweg 2, 2628 CD, Delft, The Netherlands

HIGHLIGHTS

- A DEM calibration strategy for binary mixture charging is presented.
- Interaction parameters between mixture components and individual components were calibrated.
- Calibration experiments used a single test to measure multiple KPIs at different velocities.
- Unknown parameters are calibrated using surrogate modeling and multi-objective optimization.
- Verification showed good model accuracy at different charging velocities.

GRAPHICAL ABSTRACT

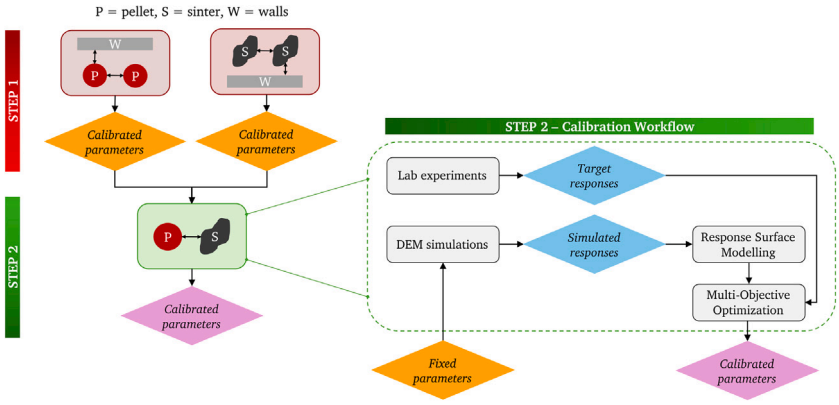

ARTICLE INFO

Keywords:
Multi-component mixture
High-velocity flow
Bulk calibration
Verification
Response surface method
Multi-objective optimization
Desirability function

ABSTRACT

In blast furnace ironmaking, a mixture of iron ore pellets and sinter is charged in layers at the furnace top, with particle velocities reaching up to ~10 m/s at the stock surface. The inherent differences in particle size, shape, and density between pellets and sinter pose challenges for maintaining a uniform mixture during this high-velocity charging, leading to segregation and uneven material distribution. This non-uniformity can negatively affect furnace efficiency and stability. Understanding segregation during charging is therefore crucial for optimizing the ironmaking process. The Discrete Element Method (DEM) can offer valuable insights, provided that the model parameters are calibrated and verified. This study presents a calibrated DEM model for a pellet–sinter mixture with a 50–50 mass ratio of both components. A novel high-velocity laboratory setup was used to simultaneously measure five different key performance indicators (KPIs) related to flow and packing behavior at various discharge heights, corresponding to different flow velocities. Calibration was performed at the highest flow velocity, representative of actual blast furnace conditions. The process involved creating response surface models for each KPI and using a multi-objective optimization approach with a desirability function to determine the model parameters. A step-wise calibration strategy was employed, first optimizing pellet and sinter interaction parameters individually, followed by calibration of the pellet–sinter interaction parameters. This approach proved effective, as the calibrated model accurately reproduced experimental data. Results also suggest that the calibration outcome is flow-invariant in this setup, with the model successfully predicting flow and packing behavior at lower discharge heights.

* Corresponding author.
E-mail address: raisaroeplal@gmail.com (R. Roeplal).

https://doi.org/10.1016/j.powtec.2025.121382
Received 21 February 2025; Received in revised form 30 May 2025; Accepted 7 July 2025
Available online 7 August 2025

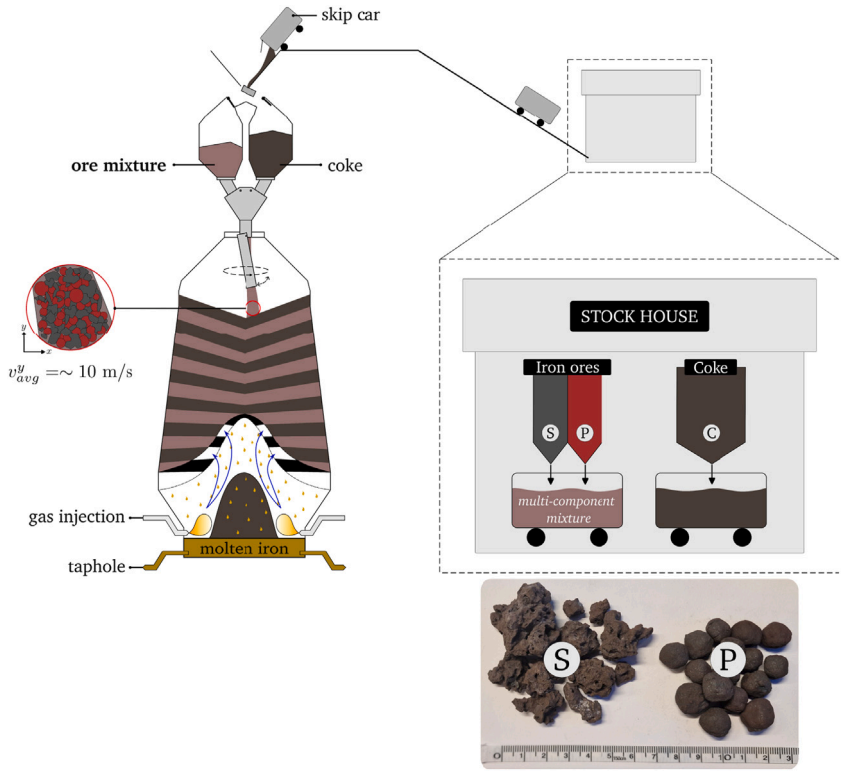

Fig. 1. Illustration of pellet–sinter mixture charging to the furnace and the bunker loading process using skip cars.

1. Introduction

A blast furnace is a large-scale industrial reactor designed to transform raw materials into liquid iron through a combination of thermal and chemical processes. It operates as a counter-current reactor, where a descending packed bed of raw materials, collectively referred to as the "burden", interacts with an ascending flow of hot gas. The burden consists of an *ore mixture*, primarily including pellets and sinter, along with coke. As illustrated in Fig. 1, these materials are loaded into the top bunkers using skip cars and subsequently charged through a rotating chute. The chute gradually reduces its inclination before rotating again, forming alternating layers of the ore mixture and coke within the packed bed. At the bottom of the furnace, a pressurized blast of hot gas is injected, initiating a series of mostly endothermic reactions as it rises through the bed. These reactions lead to the reduction and melting of the iron contained in the ore particles, ultimately collecting as molten iron at the bottom of the furnace.

For many years, researchers have pointed out that the permeability distribution of the packed bed determines the efficiency of iron extraction process [1]. Uneven permeability can cause stability issues and increase coke consumption to sustain combustion efficiency. The permeability of the bed is generally influenced by its configuration, *i.e.*, the arrangement of materials after charging. Specifically, uniform bed permeability is achieved through a homogeneous distribution of materials across the layers. Given the simultaneous variation in particle size, density, and shape between pellets and sinter, segregation of the ore mixture is anticipated during the charging process. This segregation can significantly affect the homogeneity of the ore layers. However, the extent of segregation is difficult to quantify in real-time due to the extreme conditions within the blast furnace. The Discrete Element Method (DEM) has become a valuable tool for simulating the blast furnace charging process, providing insights into particle behavior during operation. DEM employs contact models to predict interactions between particles, material types, and the furnace walls. These simulations offer critical understanding of how particle interactions influence burden distribution and segregation. However, the accuracy of these predictions is highly dependent on the model parameters, which must be determined to ensure that the model's predictions match real-world observations.

Determining DEM model parameters is inherently challenging, as no universal value exists for each particle due to the variability within materials. A practical approach is bulk calibration, where parameters are adjusted to align simulated bulk behavior with experimental data. Despite the widespread use of DEM in blast furnace simulations, model calibration practices still face several challenges [1]. For instance, the highest particle velocity in blast furnaces can reach 10–15 m/s at low chute angles, yet most calibration tests are conducted at much lower velocities. This raises concerns about the ability of existing models to accurately capture high-velocity behavior. Furthermore, calibration often relies on a single performance indicator, such as the angle of repose, which may not provide a unique combination of parameters that can replicate experimental bulk behavior [2]. Another major limitation is the treatment of interaction parameters between different materials, such as pellets and sinter. These parameters are often assumed rather than calibrated, introducing uncertainty into the modeling of mixture behavior. This is particularly concerning, as we previously demonstrated that pellet–sinter interaction parameters significantly influence the segregation behavior of the mixture during high-velocity charging [3].

In light of these limitations, the objective of this work is twofold. First, to calibrate the mixture model systematically at representative charging velocity, ensuring that a unique solution is found to the large set of model parameters. Secondly, to investigate to what extent a model calibrated at a certain velocity is capable of predicting material behavior at other velocities. To achieve these objectives, we employ a novel high-velocity calibration setup that characterizes flow and packing behavior using multiple key performance indicators (KPIs) across a range of velocities, with the highest velocity approximating industrial-scale furnace conditions. It must be noted that effects such as particle breakage, which may occur at high velocities, are not considered in

this study, as degradation phenomena would require more advanced models and dedicated calibration beyond the current scope.

This paper is organized as follows. Section 2 introduces a step-wise calibration strategy, where individual pellet and sinter parameters are first calibrated at the highest velocity, followed by the calibration of pellet–sinter interaction parameters. We describe the calibration process, which involves response surface modeling of the KPIs using DEM data, followed by a multi-objective optimization approach to determine parameter values that best match experimentally measured KPI values. Section 3 presents the results from lab experiments, and the calibration process, along with a verification step at different flow velocities. Finally, Section 4 summarizes the key findings and outlines potential directions for future research.

This work makes three key contributions to the calibration of ore mixture models for blast furnace charging. First, it presents a systematic calibration approach that accounts for both individual pellet and sinter interaction parameters as well as their mutual interaction parameters, ensuring a unique set of model parameters through the use of multiple KPIs. Second, it employs a carefully designed experimental setup that realistically replicates blast furnace flow conditions while enabling the simultaneous measurement of multiple KPIs. To our knowledge, such a setup has not yet been reported in blast furnace-related literature. Finally, this work introduces a two-step calibration strategy that reduces the number of required KPIs by first calibrating individual pellet and sinter parameters at high velocity before calibrating their interaction parameters. This structured approach streamlines the calibration process and is expected to be broadly applicable to DEM-based mixture model calibration beyond the blast furnace context.

2. Calibration method

2.1. Calibration and verification strategy

In our previous work [1], we demonstrated that DEM models for blast furnace charging are commonly developed using the Hertz-Mindlin contact model combined with rolling model C. These models have proven effective for blast furnace materials, which are coarse and free-flowing by nature. Fig. 2 summarizes the five different interactions occurring between particles and their surroundings in a DEM-based ore mixture model. When employing the Hertz-Mindlin model alongside rolling model C, these interactions are characterized by the static friction coefficient (μ_s), rolling friction coefficient (μ_r), and restitution coefficient (e). Hence, a complete ore mixture model requires a total of 15 parameters to be calibrated – a significant number. Proper calibration practices require one KPI per parameter, meaning that directly calibrating the entire mixture model would necessitate a wide range of KPIs.

To address this challenge, a step-wise calibration approach is proposed, as illustrated in Fig. 3. The idea is to start by calibrating the complete set of interaction parameters associated with the pellet and sinter models, *i.e.*, the particle–particle (P–P/S–S) *and* particle–wall (P–W/S–W) interaction parameters. Once calibrated, their values remain fixed and are used as inputs for the second calibration step, in which the pellet–sinter interaction parameters in the mixture model are calibrated. Since the pellet and sinter models each require six interaction parameters, the majority of parameters (12 out of 15) are determined during the first calibration step. By decomposing the calibration process in this way, the number of required KPIs for a unique solution is significantly reduced, from 15 to 6, thereby simplifying the overall calibration procedure.

In this work, a hopper discharge test with subsequent heap formation (shown schematically in Fig. 4) is employed as the calibration experiment. Given the need to calibrate multiple parameters at each step, the setup was specifically designed to enable the simultaneous measurement of multiple KPIs in a single test. The discharge height H is an operational variable in this setup, which can be adjusted up to

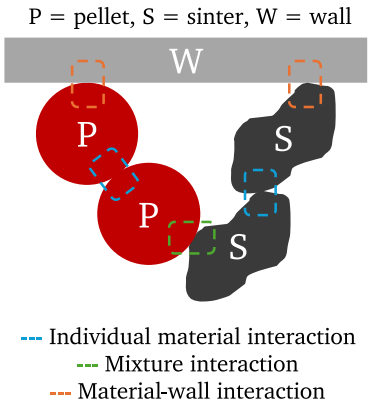

Fig. 2. Overview of the interactions in a DEM simulation involving a binary mixture of pellets and sinter particles.

a maximum value of $H = 4.665$ m to achieve different flow velocities. The experiments are conducted at $H = [1\ 3\ 4.665]$ m, corresponding to flow velocities of $v =\sim [4.4\ 7.7\ 9.6]$ m/s at the plate, as estimated using a free-fall calculation. Varying the flow velocity allows for an examination of its potential impact on the calibration results. Table 1 presents a summary of the experiments, listing the materials tested at each discharge height. The highest flow velocity of 9.6 m/s, achieved at $H = 4.665$ m, closely matches the velocity observed at the blast furnace stock level during charging [1]. Thus, the models are calibrated at this configuration. After calibrating the pellet and sinter models, an initial verification is conducted at $H = 4.665$ m to confirm the calibration outcome. The calibrated models are then further tested at $H = 1$ m and $H = 3$ m to evaluate whether re-calibration is needed at different flow velocities. Due to time constraints, the verification at $H = 1$ m and $H = 3$ m is performed only for the pellet and sinter models.

2.2. Calibration parameters and targets

The calibration experiment facilitates the measurement of five KPIs that capture material flow and packing behavior:

- KPI 1: the hopper discharge time (t_d)
- KPI 2: the heap mass (m_h)
- KPI 3: the 2D heap contour (front view)
- KPI 4: the heap center height (H_c)
- KPI 5: the heap porosity (ϕ_h)

Traditionally, the heap shape is characterized using the angle of repose, but this metric becomes less reliable at the high discharge velocities used in this work, leading to flattened heap tops as will be shown later in Section 3. Determining the angle of repose is straightforward for heaps with a distinct peak; however, the flattening of heap tops becomes more pronounced with increasing discharge height, introducing subjectivity in measuring the angle of repose. It will also be shown that the angle of repose shows a lack of sensitivity to variations in discharge height, while the flattened tip is sensitive to the discharge height. This indicates that the angle of repose alone does not sufficiently capture the heap shape. Since one of the objectives of this study is to evaluate whether a model calibrated for specific flow conditions can accurately predict material behavior under different conditions, it is essential to select KPIs that can distinguish between flow regimes. Therefore, we use the entire heap contour as a calibration target, providing a more comprehensive and reliable alternative to the angle of repose.

While the ideal KPI for calibrating a high-velocity DEM model designed to predict mixture segregation would be the segregation index, this approach would require a larger experimental setup with significantly more material, increasing complexity and time. Instead, we focus

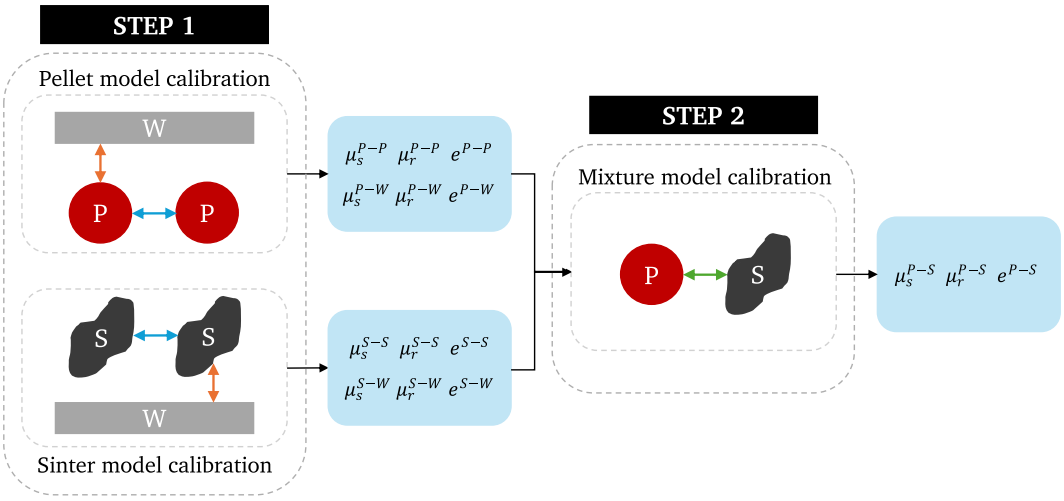

Fig. 3. Step-wise strategy for calibrating a pellet–sinter mixture model. Abbreviations: P = pellet, S = sinter, W = wall, μ_s = sliding friction coefficient, μ_r = rolling friction coefficient, e = restitution coefficient.

Table 1
Experimental setup configurations for tests with pellet, sinter, and the pellet–sinter mixture (50/50). Differences in configurations are based on the discharge height and, consequently, the flow velocity achieved at the plate.

Material	Configuration		
	H = 1 m v =~ 4.4 m/s	H = 3 m v =~ 7.7 m/s	H = 4.665 m v =~ 9.6 m/s
Pellet	verification	verification	calibration + verification
Sinter	verification	verification	calibration + verification
Mixture	–	–	calibration + verification

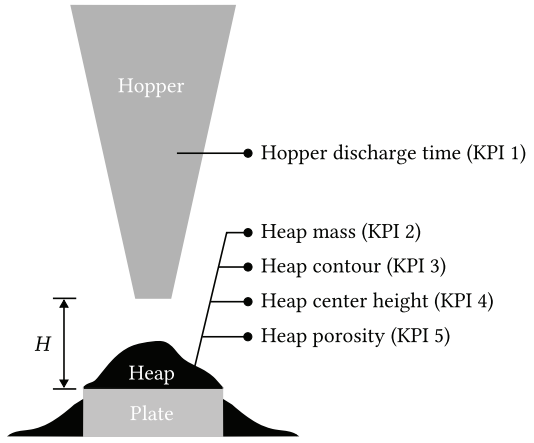

Fig. 4. Simplified representation of the setup used in calibration experiments, highlighting the KPIs that can be measured.

on the five aforementioned KPIs, as prior studies [4–8] demonstrate that calibrating based on bulk flow behavior is sufficient to develop reliable segregation models.

Despite the use of these five KPIs, the calibration process faces the challenge of an underdetermined system, as the pellet and sinter models each include six parameters. To resolve this, we fix the particle–wall restitution coefficient in the pellet and sinter models (e^{P-W} and e^{S-W}, respectively) based on values reported in the literature, reducing the parameter space to five adjustable variables per model. This approach ensures that the remaining parameters can be effectively calibrated using the available KPIs, providing a systematic and reliable foundation for model development.

2.3. Calibration workflow

Following the step-wise strategy outlined in Fig. 3, the calibration process is conducted separately for the pellet, sinter, and mixture models. The workflow presented in Fig. 5 details the steps involved in this process, which are applied to each model individually. The underlying principle of the method is that by predicting how the KPIs behave across the entire parameter space, we can identify the optimal combination of parameter values required to match the experimentally measured KPIs in our DEM simulation. This involves minimizing the difference between the simulated and measured KPI values, effectively framing the calibration as an optimization problem. This section provides a detailed explanation of each step.

2.3.1. Lab testing

Experimental setup and procedures

The experimental setup is shown in Fig. 6, with its primary components outlined below; key elements are italicized for easy identification in the figure. To contain dust generated during high-velocity discharge tests, the setup is enclosed within a laboratory *enclosure*, which is connected to a dust extraction system (not shown in Fig. 6) to remove airborne particles from the test area. The *hopper* (with key dimensions shown in Fig. 7) is mounted to an *overhead crane*, enabling it to be positioned above the *container* at adjustable discharge heights H, up to a maximum of H = 4.665 m. The hopper's outlet valve (not shown in Fig. 7) is remotely controlled to open once the hopper is positioned at the desired height H. For stability, a *hopper guide* is attached to the hopper to restrict lateral movement. This guide fits securely into a wooden *reference frame* fixed to the enclosure, ensuring that the hopper moves only vertically above the container.

The container is equipped with a *heap formation arrangement*, as shown in Fig. 8. The purpose of the heap formation arrangement is to facilitate the formation of a stable heap. It features a *collection plate* with

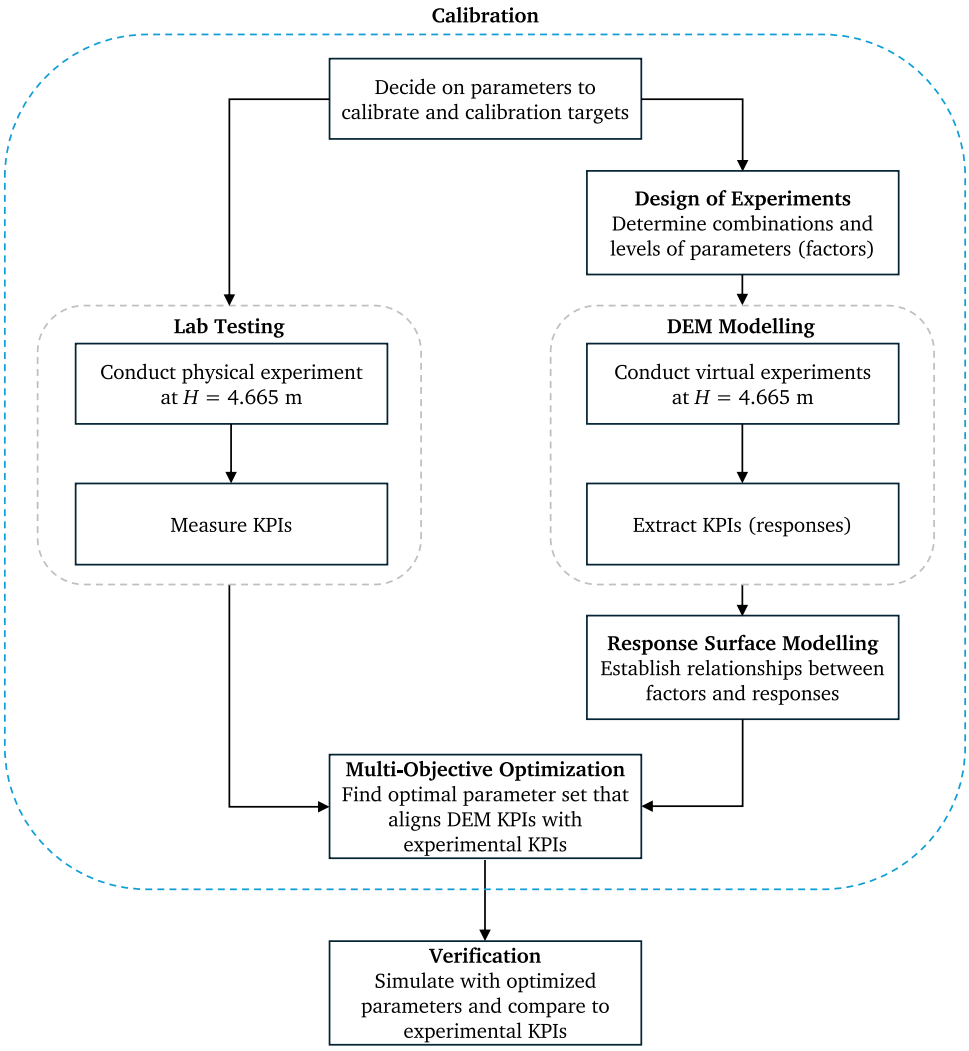

Fig. 5. Steps involved in the calibration and verification of DEM models.

side ledges that guide heap formation as material is discharged from the hopper. The plate is positioned atop a *bench scale* which measures and records the mass on the collection plate, and is equipped with a display. *Framed windows* are installed above the collection plate to confine the heap at the front and back, while any material spilling from the sides is collected in the container. The window frames are constructed from wood, the panes are made of acrylic, and all other structural components are fabricated from steel.

The test procedure is as follows. At the start of each test, the hopper is filled with material and elevated to a height H. Once positioned, the hopper is secured to a surrounding structure to ensure stability. A GoPro Hero12 is mounted in front of the hopper and turned on to record the material flow at the outlet at 240 FPS. The hopper outlet is then opened remotely, allowing material to discharge directly onto the bench scale to form a heap, and once discharge is complete, the recording is terminated.

Experimental plan

Given the calibration strategy to calibrate the pellet, sinter and pellet–sinter interactions parameters separately, we conduct experiments using pellets, sinter, and a 50/50 mass mixture of both. For each test, the hopper is filled to a fixed level, resulting in masses of 176.4 kg for pellets, 150 kg for sinter, and 160.4 kg for the mixture. Recall from Section 2.1 that H = [1 3 4.665] m for the experiments with pellets and sinter, and H = 4.665 m for experiments with the mixture. Each test case with pellets is repeated three times, and the tests with sinter and the mixture are repeated five times.

Measurement of KPIs

And the end of each experiment, the KPIs are extracted as follows:

1. *Hopper discharge time* (t_d, KPI 1)
   The total discharge time is determined through frame-by-frame video analysis using Wondershare Filmora. The start of discharge is identified as the moment the hopper outlet valve begins to move, while the end of discharge is marked when the last particle completely exits the hopper. The discharge time is then calculated as the time difference between these two events.
2. *Heap mass* (m_h, KPI 2)
   The final mass of the heap is directly read from the bench scale display.
3. *2D heap contour* (KPI 3)
   A front-view photograph of the heap is taken and processed in Matlab, as shown in Fig. 9. It must be noted that only the red-dashed portion of the photograph in Fig. 9 is analyzed, as the windowpane obstructs the left and right edges (each 0.015 m wide). Consequently, only the central 0.47 m of the heap is considered. The heap contour is extracted by converting the RGB image to a binary format, a process facilitated by the distinct contrast between the nearly uniform color of the heap particles and the green background. Initially, the extracted contour is

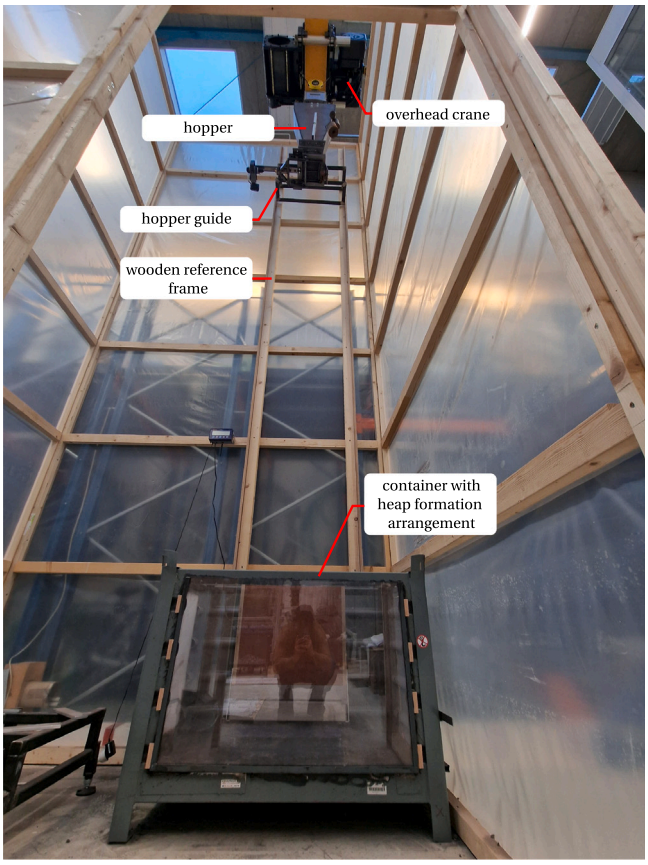

Fig. 6. Photograph of the experimental setup, highlighting its main components. The setup is housed within an enclosure designed to contain dust generated during experiments. While the enclosure can be fully closed, the door is open in this image for visibility. The dust removal system, connected to a cyclone on the left side of the enclosure, is not visible in the photograph.

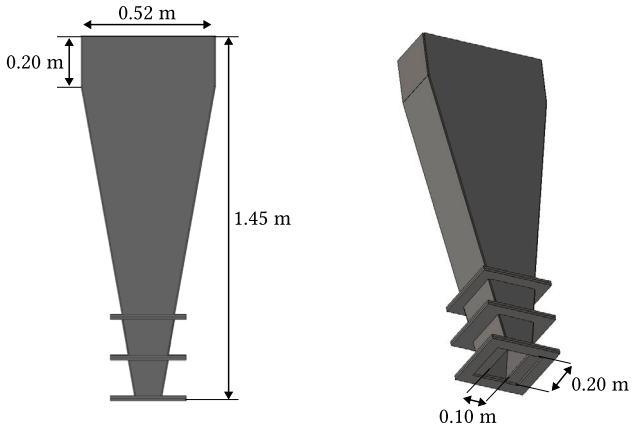

Fig. 7. Dimensions of the hopper used in the experiments.

represented in pixel coordinates. To convert the contour from pixels to physical dimensions, the x- and y-coordinates are scaled by a factor of $0.47/N$, where N is the number of pixels in x-direction.

4. *Heap center height* (H_c, KPI 4)
   After converting the heap contour to centimeter units, the center height H_c is determined in MATLAB. The center height represents the y-coordinate corresponding to $x = 0.25$ m. Since the heap contour is defined by discrete data points, interpolation is used to estimate the precise height at $x = 0.25$ m.
5. *Heap porosity* (ϕ_h, KPI 5)
   A handheld INTEL® REALSENSE™ 3D scanner captures the top surface of the heap, as shown in Fig. 10. The heap volume V_h is computed by determining the volume between the captured surface and the collecting plate. The bulk density ρ_b is then calculated as

$$\rho_b = \frac{m_h}{V_h} \tag{1}$$

   For the pellet and sinter experiments, the heap porosity is then calculated as

$$\phi_h = 1 - \frac{\rho_b}{\rho_p} \tag{2}$$

   where ρ_p is the particle density which is measured for pellet and sinter as described in Appendix A.

2.3.2. DEM virtual experiments

Simulation setup

The physical experiments are replicated in a virtual environment using ALTAIR® EDEM™ (version 2023) on the DelftBlue high-performance cluster [9] with a single GPU (NVIDIA Tesla V100S-PCIE-32 GB). The setup dimensions are consistent with the experimental configuration, and all structural components are modeled as steel. Consequently, the pellet/sinter experiments involved two material types: pellet (P)/sinter (S) particles and steel walls (W), while experiments with the mixture include all three materials. As stated in Section 2.1, the interactions between these materials are described using the Hertz-Mindlin (no-slip) contact model with an elastic–plastic spring–dashpot rolling friction model (model C). Detailed descriptions of the contact models are available in the literature [10,11], and the input parameters used in this study are summarized in Table 2.

The particle densities and size distributions for pellet and sinter were measured using 3D scanning, as described in Appendix A. The particle size distributions are presented in Fig. 12a, expressed in terms of the equivalent spherical diameter, which is derived from the measured volume distributions. The particle shapes used in the simulations are shown in Fig. 12b. Since pellets are nearly spherical in reality, they are modeled as spheres. For sinter, four randomly selected particles were scanned, and their shapes were approximated in EDEM using clumps by fitting spheres to the corresponding STL files. In general, clump accuracy improves with an increased number of spheres and the use of smaller spheres. However, both factors significantly raise computational cost. In this study, clumps were limited to a maximum of 44 spheres and the resulting clump volumes deviated by 1%–8% from the volumes of their corresponding STL templates. The Young's moduli and Poisson's ratio of all materials are taken from literature, as well as the particle–wall restitution coefficients between pellet and steel. Numerical integration is performed using the Euler scheme with a time step set to 10% of the Rayleigh time step (Δt_R), which is $\Delta t_R = 9.2\times10^{-5}$ s for simulations with pellet and $\Delta t_R = 1.1\times10^{-5}$ s for simulations with sinter and the mixture.

Each simulation consists of two main parts: the filling of the hopper and the discharging of the material into the container. A virtual volume (see Fig. 11a) is used for the generating particles using a dynamic factory. The simulation procedure is as follows. At $t = 0$ s, the factory stats generating the required amount of material. In the mixture simulations, two factories are connected to the virtual domain, each producing half of the total mixture mass. At $t = 3$ s, the hopper outlet is opened, allowing the material to flow (see Fig. 11b), and the simulation ends at $t = 15$ s, once all the material has settled in the container.

Design of Experiments

In the DEM simulations, μ_s, μ_r, and e values are allowed to vary between 0 and 1, defining the parameter space for calibration. The Box–Behnken Design (BBD) [14] was employed as an efficient and robust method to explore how the KPIs vary across the parameter space.

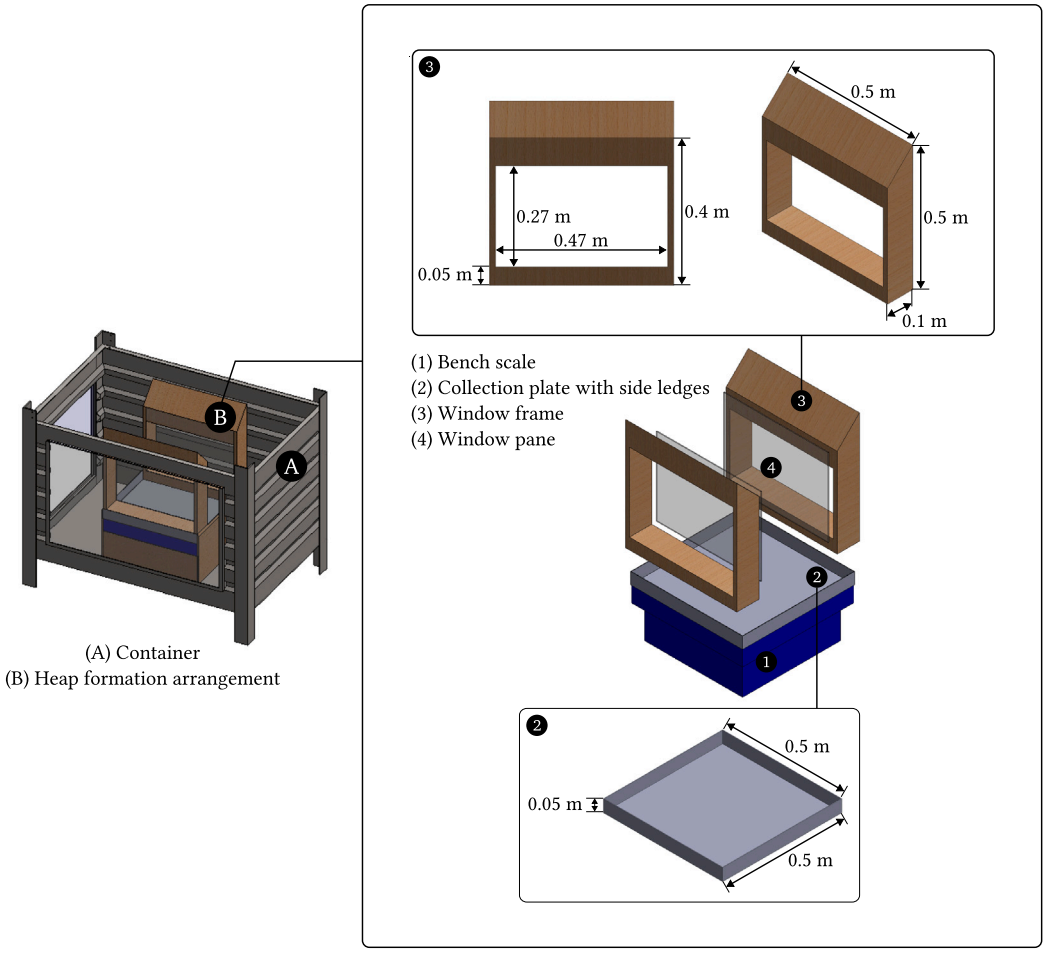

Fig. 8. Dimensions of the heap formation setup used in the experiments.

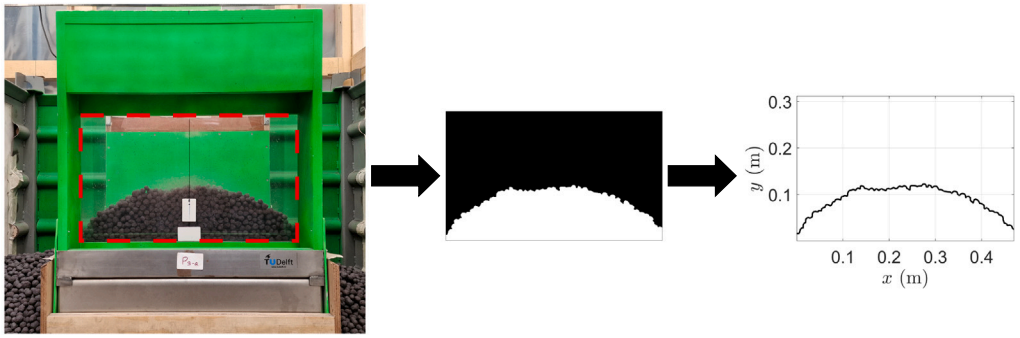

Fig. 9. Illustration of how the heap contour is extracted at the end of an experiment. The example shown is from a pellet experiment, with the same methods applied to sinter and mixture experiments.

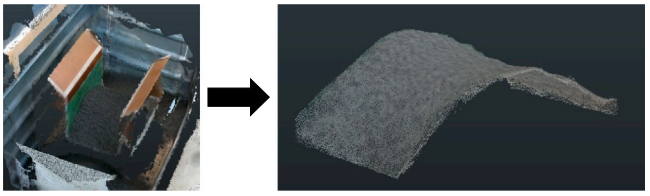

Fig. 10. Illustration of how the heap volume is extracted at the end of an experiment. The example shown is from a pellet experiment, with the same methods applied to sinter and mixture experiments.

BBD is particularly advantageous as it enables accurate estimation of linear, interaction, and quadratic effects of parameters (factors) while minimizing the number of experimental runs required [15]. In this design, each factor is assigned three coded levels: −1 (low), 0 (medium), and 1 (high). The factors and their corresponding levels in each model are detailed in Table 3. For each model, one center point was used per factor, leading to 45 runs for the pellet and sinter models, and 15 runs for the mixture model. The experimental design diagrams (EDDs) are presented in Appendix B. Each run in the EEDs was repeated three times.

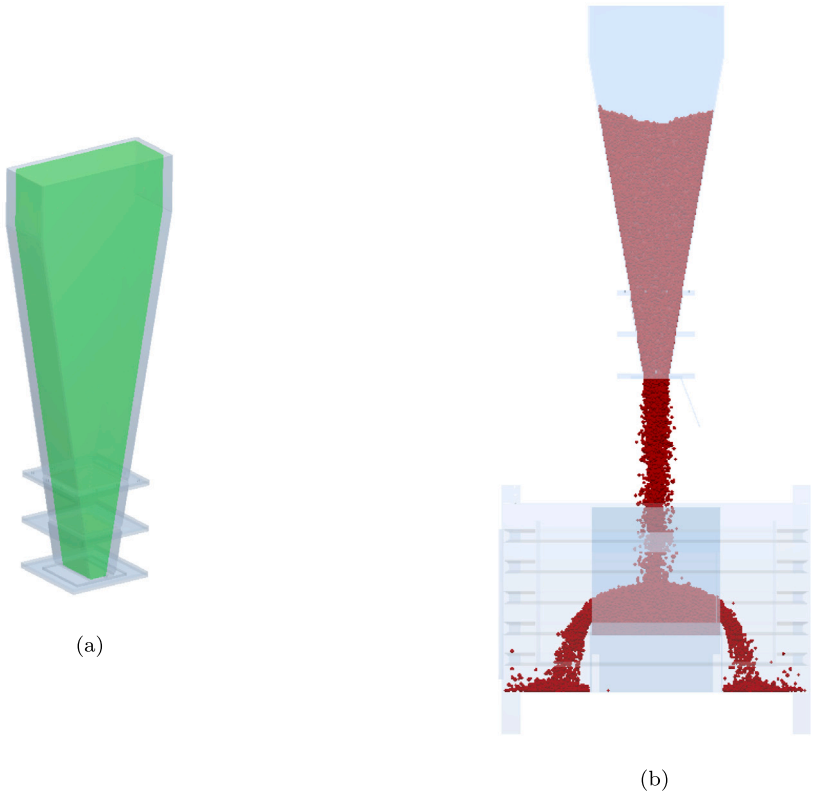

Fig. 11. Schematic of a pellet simulation setup showing (a) the virtual volume used for generating the required amount of materiel in the hopper and (b) the hopper discharging onto the bench scale.

Table 2
Hertz-Mindlin model parameters used in this work. Abbreviations: P = pellet, S = sinter, W = wall, t.b.d. = to be determined.

Parameter (symbol)		Pellet (P)	Sinter (S)	Steel wall (W)
Particle size distribution		see Fig. 12a		N/A
Particle shape		see Fig. 12b		N/A
Density (ρ) [kg/m^3]		3602	3449	7800 [12]
Poisson's ratio (ν)		0.25 [13]	0.25 [13]	0.30 [12]
Young's modulus (E) [Pa]		2.5×10^8 [13]	2.5×10^8 [13]	5.2×10^{11}
Restitution coefficient (e)	P	t.b.d.	t.b.d.	0.64 [12]
	S	t.b.d.	t.b.d.	0.40 [12]
Static friction coefficient (μ_s)	P	t.b.d.	t.b.d.	t.b.d.
	S	t.b.d.	t.b.d.	t.b.d.
Rolling friction coefficient (μ_r)	P	t.b.d.	t.b.d.	t.b.d.
	S	t.b.d.	t.b.d.	t.b.d.

Table 3
Factors and levels used in the Box–Behnken design. Abbreviations: P = pellet, S = sinter, W = wall, μ_s = sliding friction coefficient, μ_r = rolling friction coefficient, e = restitution coefficient.

Model	Factors (coded)	Factor levels		
		−1 *(low)*	*0 (mid)*	*1 (high)*
Pellet model	e^{P-P} (X_1)	0.1	0.5	0.9
	μ_r^{P-P} (X_2)	0.0	0.45	0.9
	μ_s^{P-P} (X_3)	0.1	0.5	0.9
	μ_r^{P-W} (X_4)	0.0	0.45	0.9
	μ_s^{P-W} (X_5)	0.1	0.5	0.9
Sinter model	e^{S-S} (X_6)	0.1	0.5	0.9
	μ_r^{S-S} (X_7)	0.0	0.45	0.9
	μ_s^{S-S} (X_8)	0.1	0.5	0.9
	μ_r^{S-W} (X_9)	0.0	0.45	0.9
	μ_s^{S-W} (X_{10})	0.1	0.5	0.9
Mixture model	e^{P-S} (X_{11})	0.1	0.5	0.9
	μ_r^{P-S} (X_{12})	0.0	0.45	0.9
	μ_s^{P-S} (X_{13})	0.1	0.5	0.9

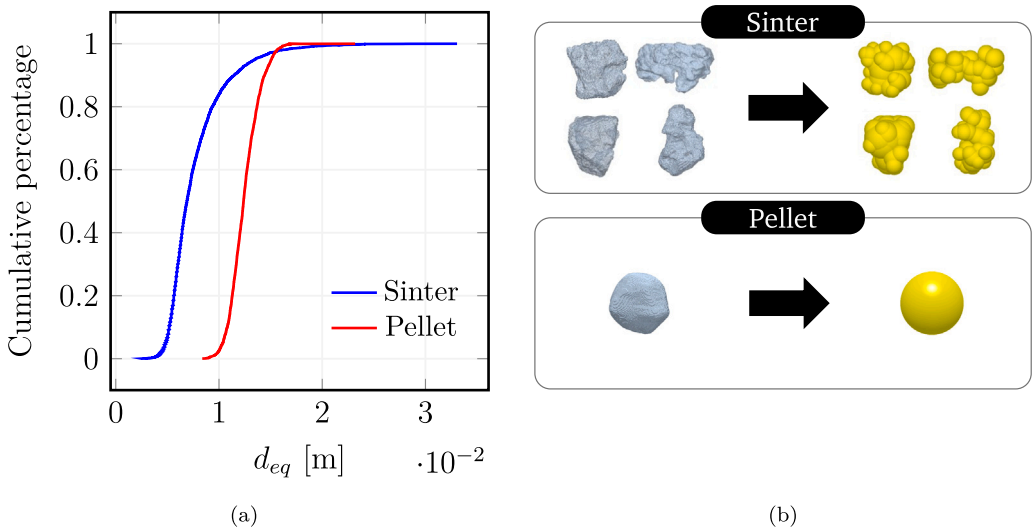

Fig. 12. Morphological features of pellet and sinter particles: (a) Cumulative particle size distributions and (b) particle shapes.

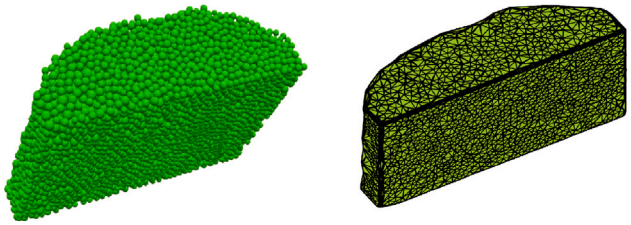

Fig. 13. Visualization of the STL of a pellet heap (left) and the *alphaShape* created using the STL vertices (right).

Extraction of KPIs

At the end of each simulation, all five KPIs are extracted from simulation data in MATLAB. In EDEM, the maximum y-position of particles in the flow is recorded every 0.01 s, enabling straightforward determination of the hopper discharge time by identifying the time step at which the maximum y-position falls below $y = H$ meters after the discharge valve is opened. Additionally, the positions of individual particles at the final time step are analyzed to identify those within the bench-scale container. Knowing the mass of each particle, the total mass on the bench scale is calculated. To determine heap porosity, the bulk heap volume is required, which is obtained by exporting the heap geometry as an STL file at the end of the simulation. This STL file, representing particles as triangular surface meshes, is imported into MATLAB. Using the *alphaShape* tool, a bounding volume is constructed from the triangle vertices (see Fig. 13), allowing for the computation of the heap's bulk density and porosity based on Eqs. (1) and (2). The heap contour and center height are determined using the same method as in the experimental counterpart, based on a front-view image of the heap.

2.3.3. Response surface modeling

Response surface modeling is a statistical method used to identify and optimize the relationships between key factors and targeted responses. The factors are the interaction parameters μ_s, μ_r, and e and KPI 1–5 serve as the calibration targets, which we aim to use as response variables. For the pellet and sinter models, which involve five factors, we develop five response surface models (RSMs) to obtain a set of equations that result in a unique solution. The mixture model, which includes only three factors, requires only three RSMs, using KPI 1–3 as the response variables. Fig. 14 provides a summary of the three models to calibrate, along with their respective factors and responses.

Since responses must be measurable and expressed as numerical values, KPIs 1, 2, 4 and 5 can be directly used as response variables. However, KPI 3 (heap contour) must be transformed into a single value to serve as a response variable. To achieve this, we quantify the similarity between the simulated heap contour and the experimental heap contour as the response variable corresponding to KPI 3. This can be done using the mean squared error (MSE) between the experimental heap height and simulated height at specific values of x, which is calculated by

$$MSE = \frac{1}{N}\sum_{i=1}^{N}\left[y^s(x_i) - y^e(x_i)\right]^2 \tag{3}$$

where x_i is the horizontal position, $y^s(x_i)$ and $y^e(x_i)$ are the height of the pile at position x_i in the simulation and experiment, respectively, and N is the total number of heap contour points used for the comparison. Fig. 15 illustrates this concept with $N = 11$, in our calculations we use $N = 100$.

The RSMs are constructed by fitting mathematical equations to the simulation data, establishing relationships between factors and responses. The fitting process is performed in R-STUDIO. Starting with a linear model and sequentially adding higher-order interactions, we determined the best fitting regression model for each response variable. The accuracy and reliability of the models are evaluated using statistical metrics such as adjusted R^2 and lack-of-fit (LoF) tests.

2.3.4. Multi-objective optimization

RSMs provide a set of equations that describe how the responses (KPIs) change in relation to the factors (parameter values). For each KPI, the objective is to identify the combination of factors that yields an RSM-predicted value as close as possible to the experimental measurement. As multiple KPIs are involved, the task becomes one of finding the optimal factor combination that satisfies all objectives, which leads to a multi-objective optimization problem. The desirability function approach [16,17] is widely used for handling such problems, as it converts multiple response objectives into a single composite desirability score. This method assigns a desirability score to each response based on predefined criteria, typically ranging from 0 (undesirable) to 1 (fully desirable). By maximizing the overall desirability function, the optimal factor settings that best satisfy all KPIs can be identified. To identify optimal parameter values, a multi-objective optimization was performed using the desirability function approach. This technique allowed for the simultaneous optimization of multiple responses by assigning weights and combining them into a single desirability score.

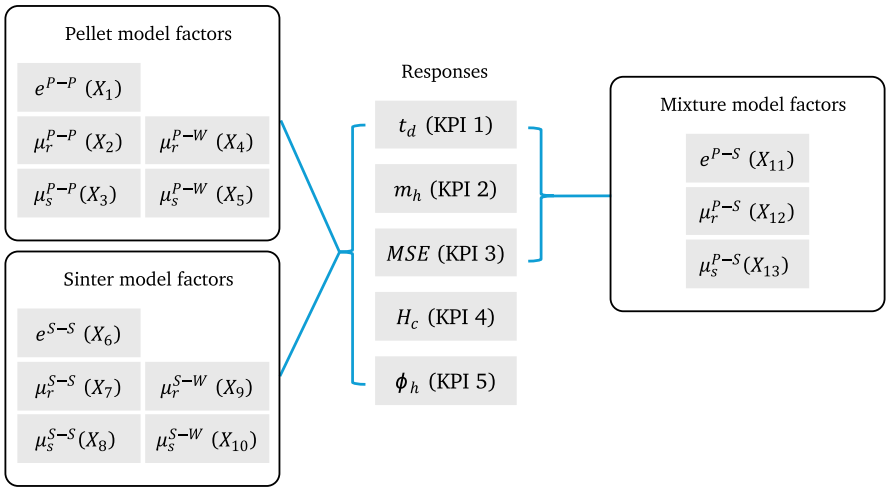

Fig. 14. Overview of factors $(X_1, \ldots, X_{13})$ and responses (KPIs) for each model.

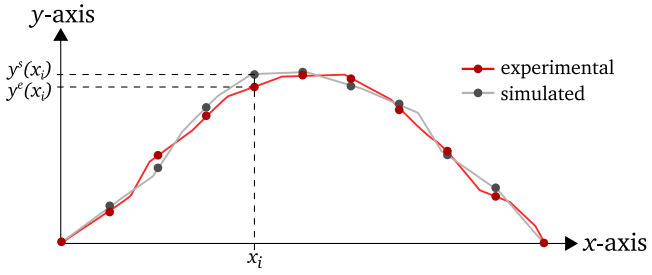

Fig. 15. Graphical representation of the comparison between simulated and experimental heap contours using $N = 11$ contour points.

The parameters that maximized the overall desirability were selected as the optimal calibration parameters for the DEM model.

The steps involved in the desirability function approach are briefly outlined as follows for N factors and M responses. First, a set of sample points (grid) is generated, corresponding to different combinations of the factors $(X_1, \ldots, X_N)$. Using the response surface models, the response Y_i^p is then computed for each of these sample points. We determine the relative difference between the predicted response Y_i^p and its experimental counterpart Y_i^e as

$$Z_i = \text{abs}\left(Y_i^p - Y_i^e\right)/Y_i^e \tag{4}$$

and transform the calculated value into a "desirability" score (d_i) as [17]

$$d_i = \begin{cases} 1, & \text{if } Z_i \le L, \\ \left(\frac{U-Z_i}{U-L}\right)^s, & \text{if } L < Z_i \le U, \\ 0, & \text{if } Z_i > U. \end{cases} \tag{5}$$

where s is a shape parameter controlling the steepness of the desirability curve and U and L are the upper and lower limits of Z_i, respectively. Note that d_i is an array containing desirability values across all sample points for response i ranging from 0 (undesirable) to 1 (highly desirable). The individual desirability arrays corresponding to each response variable are then aggregated into a single, overall desirability score (D), which is determined by [17]

$$D = \prod_{i=1}^{M} \left(d_i^{w_i}\right)^{1/\sum w_i} \tag{6}$$

where w_i is the weight assigned to the ith response, reflecting its relative importance. Finally, D is maximized to identify the optimal solution across all objectives. In this work, we set $s = 1$ to obtain a linear desirability curve, $w = 1$ to assign equal importance to all responses and use $L = 0.00$ and $U = 0.05$ for each response, indicating that a maximum relative difference of 5% is considered acceptable.

Fig. 16 illustrates the steps described in applying the desirability function approach. This figure pertains to the calibration of the pellet and sinter models, where five response surface models are used for optimization according to Fig. 14. The same approach is applied to the calibration of the mixture model; however, only three response surface models are utilized.

Table 4
Measured values of the hopper discharge time (t_d) for experiments with pellet, sinter and the pellet–sinter mixture (50/50). Results are presented as mean values with associated standard deviations, based on N experiments for each case: $N = 10$ for sinter experiments, $N = 5$ for pellet and mixture experiments.

Material	Mass in hopper (kg)	t_d (s)
Pellet	176.4	5.24 ± 0.28
Sinter	150.0	4.62 ± 1.00
Mixture	160.0	4.40 ± 0.31

3. Results

3.1. Experimental results

Table 4 presents the measured hopper discharge times for pellets, sinter, and the pellet–sinter mixture. On average, pellets take the longest to discharge; however, the sinter exhibits a relatively large standard deviation in discharge time. This variability is likely caused by interactions between the highly non-spherical sinter particles and the hopper walls, which are not perfectly smooth due to welds and grooves from its construction. Fig. 17 illustrates this with a photograph taken at the end of a sinter charging test, showing sinter particles stuck at the outlet, where their sharp edges latch onto the grooves.

Fig. 18 presents the heap mass formed on the bench scale for pellets, sinter, and their mixture at different discharge heights (H). For both pellets and sinter, the heap mass decreases as H increases, which aligns with expectations: greater discharge heights lead to higher impact velocities, causing more material to rebound from the heap. As shown in Fig. 19, the heap peak flattens with increasing H, a trend observed for both pellet and sinter heaps. Additionally, the sinter heap becomes more asymmetric at higher H. It is important to note that although the overall heap shape changes with H, the heap angle remains relatively constant before the heap starts to flatten. This indicates that the repose angle in this setup is not highly sensitive to flow velocity, supporting

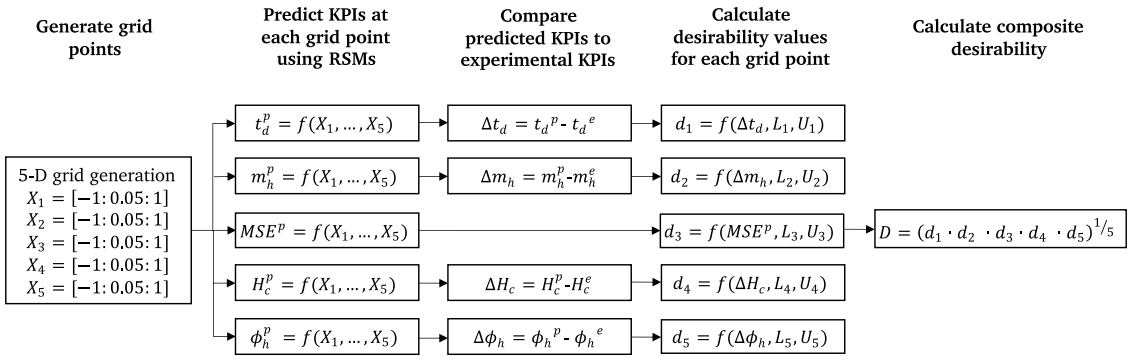

Fig. 16. Steps involved in calculating the overall desirability from the factors ($X_1, \ldots, X_{13}$) and the RSMs.

Fig. 17. Photograph taken at the end of a sinter charging experiment, showing accumulated sinter particles at the hopper outlet.

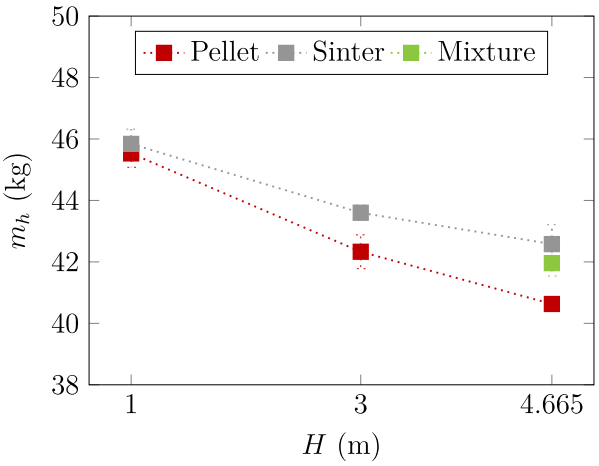

Fig. 18. Measured values of the heap mass (m_h) for all experiments, with different discharge heights (H). Error bars represent standard deviations based on N experiments for each case: $N = 3$ for pellet experiments, $N = 5$ for sinter and mixture experiments.

Table 5
Measured values of the heap center height (H_c, in cm) for all experiments, with different discharge heights (H). Results are presented as mean values with associated standard deviations, based on N experiments for each case: $N = 3$ for pellet experiments, $N = 5$ for sinter and mixture experiments.

Material	$H = 1$ m	$H = 3$ m	$H = 4.665$ m
Pellet	20.15 ± 0.31	17.79 ± 0.58	16.31 ± 0.42
Sinter	24.26 ± 0.43	20.88 ± 0.66	19.88 ± 0.45
Mixture	N/A	N/A	17.86 ± 0.54

Table 6
Measured values of the heap porosity (ϕ) for all experiments, with different discharge heights (H). Results are presented as mean values with associated standard deviations, based on N experiments for each case: $N = 3$ for pellet experiments, $N = 5$ for sinter and mixture experiments.

Material	$H = 1$ m	$H = 3$ m	$H = 4.665$ m
Pellet	0.42 ± 0.02	0.44 ± 0.02	0.47 ± 0.01
Sinter	0.48 ± 0.01	0.47 ± 0.02	0.47 ± 0.01

our decision, as discussed in Section 2.2, to refrain from using the repose angle as a calibration target.

Across all discharge heights, the sinter heap consistently retains a higher mass. Given the lower density of sinter particles, this suggests that the sinter heap's volume is consistently larger than that of the pellet heap. This observation is confirmed by Fig. 20, which compares the heap contours of the materials at different H values. The difference is likely due to the spherical shape of pellet particles, which roll more easily and are less prone to forming stable heaps compared to sinter particles under the same conditions. The heap mass of the mixture falls between that of the pellet and sinter heaps, reflecting intermediate behavior that is consistent with its composition. The heap center heights extracted from these profiles are summarized in Table 5.

Fig. 21 shows the bulk density values of pellet, sinter, and the pellet–sinter mixture. The sinter heap consistently exhibits a lower bulk density compared to the pellet heap, which can be attributed to the irregular shapes of the sinter particles. As the discharge height increases, the bulk density of the sinter heap increases, indicating a denser packing, while the opposite trend is observed for the pellet heap. This is also reflected in Table 6, which shows that the porosity of the sinter heap decreases with increasing H while the opposite is true for the pellet heap.

3.2. RSM and optimization

The simulation results based on the BBD approach are presented in Appendix C. The reported response values represent the average

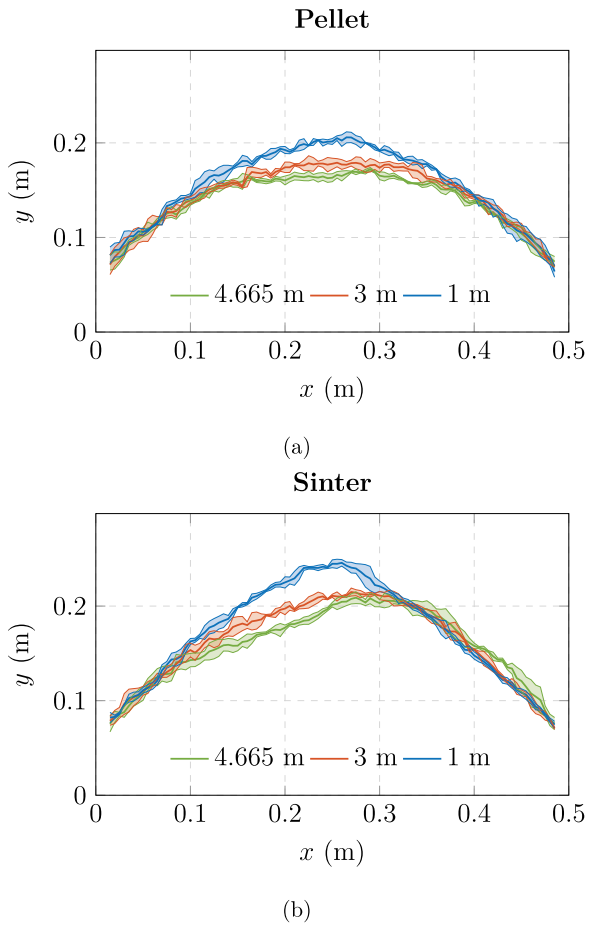

Fig. 19. Comparison of heap profiles at different heights for (a) pellet and (b) sinter.

of three replications per run. Using the data from Tables C.1–C.3, we developed response surface models (RSMs) for each response. The general form of the RSM for pellets, incorporating main effects, interaction effects, and quadratic effects of the factors $(X_1, \ldots, X_5)$, is given by

$$\begin{aligned} Y^Z = {} & A + BX_1 + CX_2 + DX_3 + EX_4 + FX_5 \\ & + GX_1X_2 + HX_1X_3 + IX_1X_4 + JX_1X_5 \\ & + KX_2X_3 + LX_2X_4 + MX_2X_5 \\ & + NX_3X_4 + OX_3X_5 \\ & + PX_4X_5 \\ & + QX_1^2 + RX_2^2 + SX_3^2 + TX_4^2 + UX_5^2 \end{aligned} \tag{7}$$

where Y represents the response variable. The RSMs for sinter follow the same structure, with the factors $X_1, \ldots, X_5$ replaced by $X_6, \ldots, X_{10}$, respectively. For the mixture system, which involves three factors (X_{11}, X_{12}, X_{13}), the general form of the RSMs is

$$\begin{aligned} Y^Z = {} & A + BX_{11} + CX_{12} + DX_{13} \\ & + EX_{11}X_{12} + FX_{11}X_{13} \\ & + GX_{12}X_{13} \\ & + HX_{11}^2 + IX_{12}^2 + JX_{13}^2 \end{aligned} \tag{8}$$

The coefficients corresponding to each RSM for pellet, sinter and the mixture are summarized in Table 7. As shown in Table 8, the models show adequate values of the statistical metrics and therefore capable of describing complex, non-linear relationships between the factors and responses.

The multi-objective optimization process was conducted to determine the optimal values of the models' parameters such that there is a maximum deviation of 5% between experimental and RSM-predicted KPI values. The optimal (calibrated) interaction parameter values for all models are summarized in Table 9. The overall desirability associated with these solutions for the pellet, sinter and mixture models were 0.51, 0.56 and 0.41, respectively.

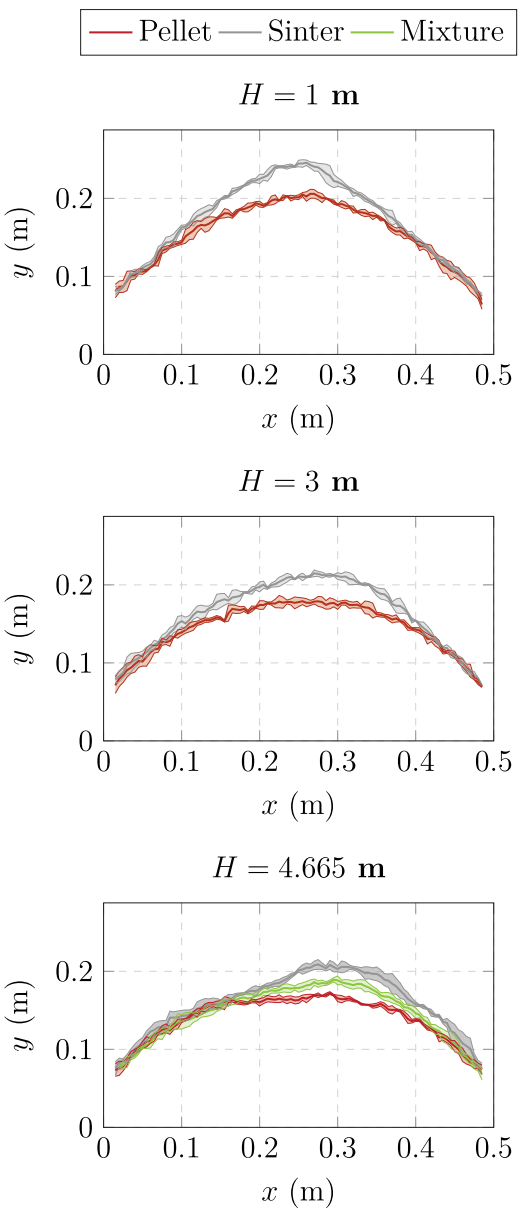

Fig. 20. Reconstructed contours of the heaps formed at different discharge heights (H). Shaded areas represent standard deviations based on N experiments for each case: $N = 3$ for pellet experiments, $N = 5$ for sinter and mixture experiments.

3.3. Verification

The parameter values listed in Table 9 are applied to our DEM models with a heap height of $H = 4.665\,\text{m}$ to assess how well the simulated KPIs align with the experimental ones. Table 10 presents this comparison, demonstrating that the calibrated parameters enable the models to reproduce the experimental KPIs for pellets, sinter, and the mixture with good accuracy. The relative difference between DEM predictions and experimental values ranges from 0.02% to 5.53%, which is consistent with reported errors in the DEM literature for model calibration using response surface modeling [18–27].

Table 7
Coefficients for the general response surface model (RSM) equations for pellets, sinter, and the mixture. Eq. (7) applies to pellets and sinter, where Y represents t_d, m_h, ϕ_h, H_c and MSE. Eq. (8) applies to the mixture, where Y represents t_d, m_h and MSE.

	Pellet					Sinter					Mixture		
	t_d	m_h	ϕ_h	H_c	MSE	t_d	m_h	ϕ_h	H_c	MSE	t_d	m_h	MSE
A	4.6381	46.1048	0.4583	0.2008	0.066	4.858	44.364	0.4873	0.221	0.168	4.765	2.732	0.05
B	0	−4.6704	−0.0113	−0.0264	−0.014	0	0	−0.00837	0	−0.002	0	0	0.001
C	0.451	8.795	0.0076	0.0485	0.015	0.263	2.617	0.01197	0.021	0.036	0.18	1.983	0.01
D	0.5658	8.4458	0.0126	0.0518	−0.008	0.708	3.504	0.02938	0.037	−0.023	0.515	4.64	−0.015
E	0.1096	0	0	0	0	0.068	0	0	0	0	0	0	−0.003
F	1.2515	0	0	0	0	1.077	2.147	−0.00417	0.013	0	0	0	−0.002
G	0	−2.9496	−0.0045	−0.021	−0.029	0	0	0	0	−0.005	0.015	0.484	0.017
H	0	−0.2157	−0.0086	−0.0082	−0.024	0	0	−0.00586	0	−0.007	0	0	0
I	0	0	0	0	0	0	0	0	0	0	0	−0.661	−0.001
J	0	0	0	0	0	0	0	−0.0021	0	0	−0.236	−3.934	0.024
K	0	4.8044	0.0037	0.0309	0.022	0	0	0	0	0.044			
L	0	0	0	0	0	0	0	0	0	0			
M	0	0	0	0	0	0	0	0	0	0			
N	0	0	0	0	0	0	0	0	0	0			
O	0	0	0	0	0	0	0	5.21E−05	−0.006	0			
P	0	0	0	0	0	0	0	0	0	0			
Q	0	−3.8128	−0.0041	−0.01969	−0.008	0	0	−0.00239	0	−0.0002			
R	−0.1718	−2.4308	−0.0058	−0.0161	0.017	−0.049	−0.632	−0.00385	−0.005	−0.006			
S	−0.2993	−6.8921	−0.0067	−0.0389	0.015	−0.316	−4.677	0	−0.036	0.025			
T	−0.982	0	0	0	0	−0.007	0	0	0	0			
U	−0.0335	0	0	0	0	−0.275	−0.871	0	−0.005	0			
Z	1	1	1	1	0.384	1	1	1	1	0.222	1	1	0.343

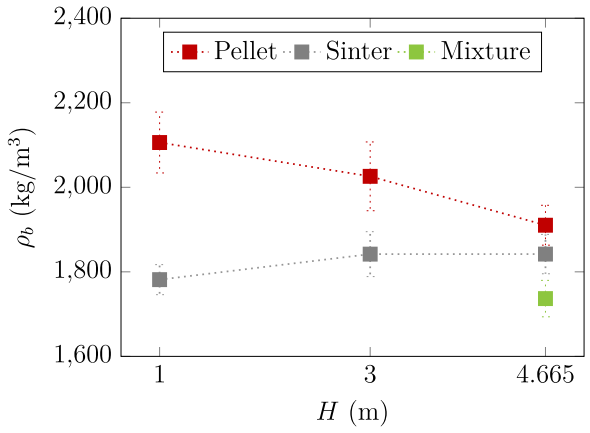

Fig. 21. Measured values of the heap bulk density (ρ_h) for all experiments, with different discharge heights (H). Error bars represent standard deviations based on N experiments for each case: $N = 3$ for pellet experiments, $N = 5$ for sinter and mixture experiments.

Table 8
Metrics showing the goodness-of-fit of the developed RSMs.

Material	RSM	LoF p-value[a]	Adj. R^2
Pellet	t_d	0.47	0.96
	m_h	0.50	0.92
	ϕ_h	0.77	0.90
	H_c	0.40	0.93
	MSE	0.16	0.63
Sinter	t_d	0.68	0.99
	m_h	0.98	0.98
	ϕ_h	0.28	0.99
	H_c	0.26	0.98
	MSE	0.48	0.63
Mixture	t_d	0.54	0.98
	m_h	0.27	0.99
	MSE	0.20	0.88

[a] Guideline [14]: $p > 0.1$

Table 9
Calibrated parameter values for pellet, sinter and the pellet–sinter mixture. Abbreviations: $p-p$ = particle–particle, $p-w$ = particle–wall.

Material model	e^{p-p}	μ_r^{p-p}	μ_s^{p-p}	μ_r^{p-w}	μ_s^{p-w}
Pellet	0.1	0.08	0.57	0.15	0.86
Sinter	0.5	0.06	0.49	0.09	0.54
Mixture	0.1	0.28	0.34	N/A	N/A

The uncertainties in the simulated heap mass and heap center height are of the same order of magnitude as those observed in the physical experiments. In contrast, the DEM-predicted porosity exhibits significantly lower variability than the experimental measurements, whereas the predicted discharge times show greater variability than those recorded in the laboratory. This discrepancy in predicted versus observed variability, despite accurate mean values, has also been reported by Fransen et al. [28]. As in their study, the mismatch is likely attributable to modeling assumptions related to particle shape. As discussed in Section 2, the high experimental variability in sinter discharge times is likely due to the complex geometries of sinter particles, particularly their sharp edges, which can interact with welds and grooves in the hopper wall. These interactions are not fully captured in the DEM model for two main reasons. First, while the clump representations used in the DEM simulations approximate the overall geometry of sinter particles, they lack sharp edges. Accurately reproducing surface roughness would require an impractically high number of constituent spheres per clump. This level of detail is not feasible with current computational resources. Second, the experimental hopper walls include imperfections that are not fully represented in the DEM geometry. As a result, additional particle–wall interactions are excluded. These modeling limitations likely contribute to the observed discrepancies in discharge time variability.

Nonetheless, the mean sinter discharge time is predicted with high accuracy. The good agreement between the calibrated DEM models and the experimentally observed behavior is further illustrated in Fig. 22. The plots highlight the overall good match between the simulated and experimentally measured heap contours for pellets, sinter, and the mixture at $H = 4.665$ m. The Concordance Correlation Coefficient (CCC), which quantifies the similarity between the simulated and experimental average heap contours, shows values greater than 0.97 in all cases, indicating a substantial match [29].

Table 10
Comparison of experimental and simulated KPI values after model calibration at H=4.665 meters.

KPI (unit)	Material	Exp.	Sim.	Difference
t_d (s)	Pellet	5.24 ± 0.28	4.95 ± 0.02	−5.53%
	Sinter	4.62 ± 1.00	4.65 ± 0.05	+0.65%
	Mixture	4.40 ± 0.31	4.58 ± 0.03	+4.09%
m_h (kg)	Pellet	40.63 ± 0.21	38.63 ± 0.21	−4.92%
	Sinter	42.58 ± 0.63	41.70 ± 0.58	−2.07%
	Mixture	41.96 ± 0.42	41.33 ± 0.41	−1.50%
H_c (cm)	Pellet	16.32 ± 0.41	16.08 ± 0.30	−1.47%
	Sinter	19.88 ± 0.45	19.88 ± 0.50	+0.02%
	Mixture	17.86 ± 0.54	18.48 ± 0.27	+3.47%
ϕ_h (–)	Pellet	0.47 ± 0.01	0.451 ± 0.001	−4.04%
	Sinter	0.47 ± 0.01	0.474 ± 0.004	+0.85%

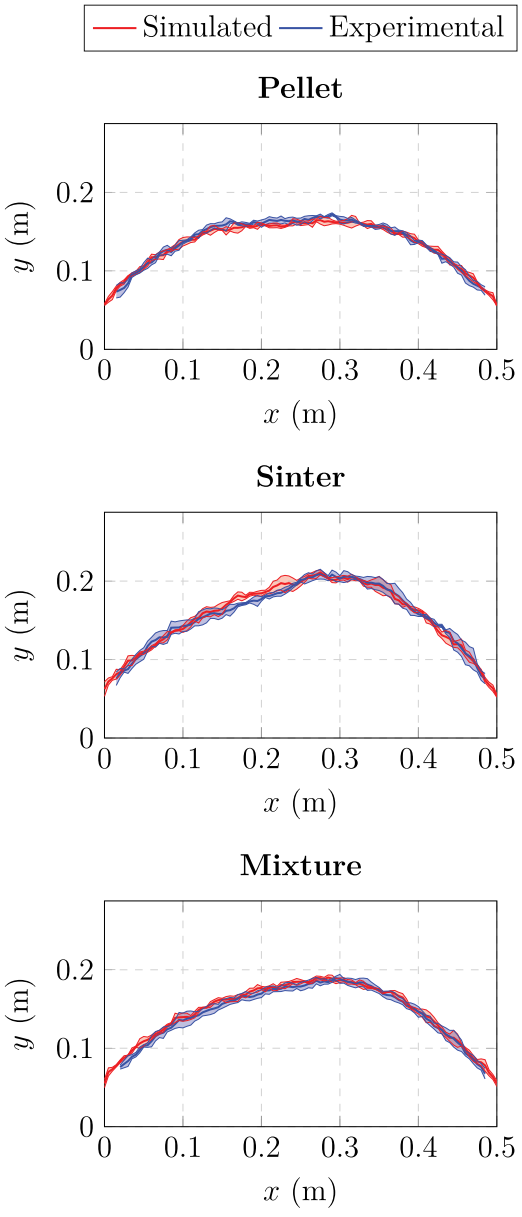

Fig. 22. Comparison of simulated and experimental heap profiles for different materials at different heights. Shaded areas represent the standard deviation with $N = 3$ for experiments with pellet and $N = 5$ for experiments with sinter and the mixture.

To assess whether our pellet and sinter models, calibrated at high velocity (~ 9.6 m/s), remain valid for lower flow velocities, we tested the calibrated parameters in simulations with $H = 1\,\text{m}$ and $H = 3\,\text{m}$, corresponding to estimated velocities of ~ 4.4 and ~ 7.7 m/s, respectively. According to Table 11, the relative differences between simulated and experimental KPI values is still in the same order of magnitude as the differences observed at $H = 4.665$ m. Considering the heap shape, Fig. 23 demonstrates that the simulated and experimental heap contours match well for both pellet and sinter at $H = 1\,\text{m}$ and $H = 3\,\text{m}$. These results suggest that, for this system and these materials, the calibration outcome is flow invariant.

4. Conclusions and recommendations

This study introduced a step-wise calibration strategy for modeling a pellet–sinter mixture under high-velocity conditions (~9.6 m/s). A novel calibration setup was employed, enabling the simultaneous measurement of five KPIs in a single hopper discharge experiment. By adjusting the discharge height, the setup also provided control over the flow velocity. The combination of this calibration strategy and experimental setup allowed us to achieve two key objectives: (1) ensuring a unique calibration solution by assigning one KPI to each parameter and (2) assessing the validity of the calibrated models across different operating conditions by verifying their performance at lower flow velocities (~ 7.7 and 4.4 m/s). The key conclusions and insights from this work are as follows:

- The step-wise calibration approach for mixtures proved effective, as the calibrated mixture model accurately captured the experimentally measured average KPI values at a discharge height of 4.665 m, with a maximum deviation of 5.5%. This shows that parameters calibrated for individual material models can be successfully applied to a mixture model of those materials, followed by the calibration of the interaction parameters.
- The combination of response surface methodology and the desirability function approach is a robust method for calibrating DEM models using multiple KPIs.
- Experimental results demonstrated that KPI values depend on discharge height (flow velocity). The calibrated models, developed at the highest flow velocity, successfully captured this dependency, indicating that the calibration is flow-invariant in this setup.
- Determining the angle of repose through piling is challenging in high-velocity flows, as the distinct heap peak becomes less prominent with increasing flow velocity, making it difficult to identify which regions of the heap to use for calculation. However, the steepness of the heap at both the far left and right sides seems to remain constant across different flow velocities, indicating that it could be treated as a flow-invariant KPI. Therefore, the overall heap shape is a more reliable KPI when calibrating a model for specific flow conditions.
- The calibrated models based on randomly selected sinter shapes showed strong predictive capabilities for average KPI values, both for sinter alone and for the pellet–sinter mixture. However, the model did not fully capture the experimentally observed variability, particularly in sinter discharge time. This limitation may be

Table 11
Comparison of experimental and simulated KPI values after model calibration at H=4.665 meters.

KPI (unit)	H	Material	Exp.	Sim.	Difference
m_h (kg)	1 m	Pellet	45.53 ± 0.45	42.92 ± 0.28	−5.73%
		Sinter	45.84 ± 0.45	44.58 ± 0.03	−2.75%
	3 m	Pellet	42.33 ± 0.55	40.10 ± 0.10	−5.27%
		Sinter	43.60 ± 0.25	42.66 ± 0.11	−2.16%
H_c (cm)	1 m	Pellet	20.15 ± 0.31	19.67 ± 0.08	−2.38%
		Sinter	24.26 ± 0.43	24.28 ± 0.27	+0.08%
	3 m	Pellet	17.79 ± 0.58	17.06 ± 0.31	−4.10%
		Sinter	20.88 ± 0.66	21.11 ± 0.24	+1.10%
ϕ_h (-)	1 m	Pellet	0.415 ± 0.020	0.450 ± 0.001	+8.43%
		Sinter	0.483 ± 0.010	0.484 ± 0.001	+0.21%
	3 m	Pellet	0.438 ± 0.023	0.451 ± 0.001	+2.97%
		Sinter	0.466 ± 0.015	0.479 ± 0.002	+2.79%

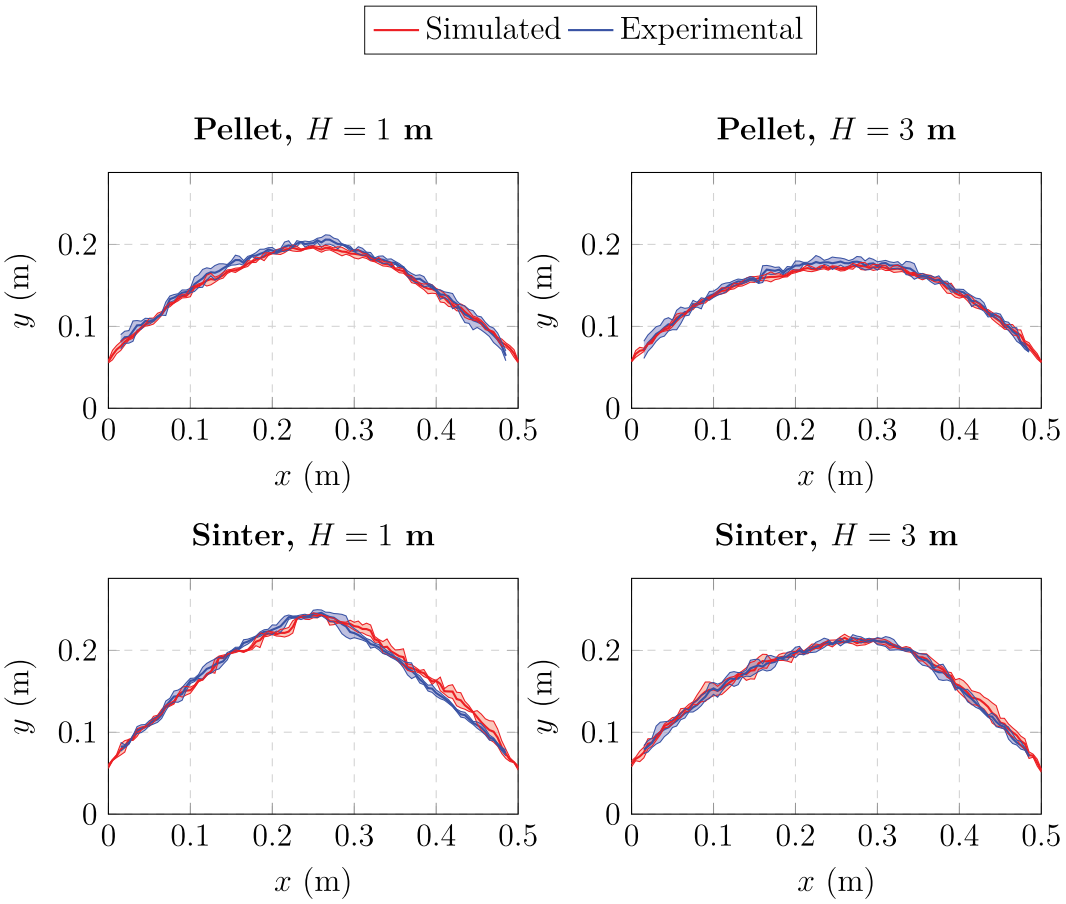

Fig. 23. Comparison of simulated and experimental heap profiles for different materials at different heights. Shaded areas represent the standard deviation with $N = 3$ for experiments with pellet and $N = 5$ for experiments with sinter and the mixture.

attributed to the selection or clump accuracy of the sinter shapes. Further investigation is needed to better understand the influence of particle shape on KPI variability and to improve predictive accuracy.

These findings demonstrate the effectiveness of the proposed calibration strategy and establish a solid basis for applying the developed mixture model to high-velocity blast furnace charging simulations. To extend the model's applicability to full-scale furnace modeling, the following directions are recommended for future work:

- Verify model performance using the segregation index: The mixture model developed in this work was not evaluated for its ability to capture segregation behavior, due to time and resource limitations. However, since the model is intended for blast furnace charging applications where segregation plays a critical role, such verification should be considered in future work.
- Develop and validate particle up-scaling strategies: The current mixture model is based on true (unscaled) particle size distributions and uses non-spherical particles represented by clumps to simulate 160 kg of ore. In contrast, real blast furnace operations involve hundreds of tonnes of material, making direct application of the current model computationally infeasible. To enable industrial-scale simulations, particle up-scaling strategies must be explored and validated against operational data to ensure reliability of the up-scaled model.
- Investigate the generalizability of the calibrated mixture model: The mixture model was calibrated for a 50/50 mass-based mixture of pellet and sinter, and the verification results confirmed its performance for this composition. A valuable direction for future

Table B.1
Experimental design diagram for establishing a pellet model, detailing the runs and corresponding factor values (X_1-X_5) for each run.

Run	X_1	X_2	X_3	X_4	X_5
1	−1	−1	0	0	0
2	−1	1	0	0	0
3	1	−1	0	0	0
4	1	1	0	0	0
5	−1	0	−1	0	0
6	−1	0	1	0	0
7	1	0	−1	0	0
8	1	0	1	0	0
9	−1	0	0	−1	0
10	−1	0	0	1	0
11	1	0	0	−1	0
12	1	0	0	1	0
13	−1	0	0	0	−1
14	−1	0	0	0	1
15	1	0	0	0	−1
16	1	0	0	0	1
17	0	−1	−1	0	0
18	0	−1	1	0	0
19	0	1	−1	0	0
20	0	1	1	0	0
21	0	−1	0	−1	0
22	0	−1	0	1	0
23	0	1	0	−1	0
24	0	1	0	1	0
25	0	−1	0	0	−1
26	0	−1	0	0	1
27	0	1	0	0	−1
28	0	1	0	0	1
29	0	0	−1	−1	0
30	0	0	−1	1	0
31	0	0	1	−1	0
32	0	0	1	1	0
33	0	0	−1	0	−1
34	0	0	−1	0	1
35	0	0	1	0	−1
36	0	0	1	0	1
37	0	0	0	−1	−1
38	0	0	0	−1	1
39	0	0	0	1	−1
40	0	0	0	1	1
41	0	0	0	0	0
42	0	0	0	0	0
43	0	0	0	0	0
44	0	0	0	0	0
45	0	0	0	0	0

research is to explore whether the same model can accurately represent other mixture compositions, thereby assessing its broader applicability, since the ore composition may vary in blast furnace operations.

Abbreviations

Abbreviation	Meaning
BBD	Box–Behnken Design
CCC	Concordance Correlation Coefficient
DEM	Discrete Element Method
EDD	Experimental Design Diagram
KPI(s)	Key Performance Indicator(s)
LoF	Lack-of-Fit
MSE	Mean-squared error
RSM(s)	Response Surface Model(s)

CRediT authorship contribution statement

Raïsa Roeplal: Writing – original draft, Software, Formal analysis, Writing – review & editing, Validation, Investigation, Conceptualization, Visualization, Methodology, Data curation. **Yusong Pang:** Supervision, Writing – review & editing. **Dingena Schott:** Writing – review & editing, Supervision.

Declaration of competing interest

The authors declare that they have no known competing financial interests or personal relationships that could have appeared to influence the work reported in this paper.

Acknowledgments

This work was carried out as part of the “Industrial Dense Granular Flows” project, which received funding from the Dutch Research Council (NWO) in the framework of the ENW PPP Fund for the top sectors and from the Ministry of Economic Affairs in the framework of the “PPS-Toeslagregeling”. The authors greatly appreciate ir. Jan van der Stel and dr. ir. Allert Adema from Tata Steel IJmuiden for arranging the substantial materials needed for the experiments and the valuable discussions in the context of the blast furnace. The technical staff at TU Delft are also gratefully acknowledged: Ed Stok and Andre van den Bosch for their contributions to the design and commissioning of the experimental setup, and Huib Zuurmond for assistance during the execution of the experiments.

Table B.2
Experimental design diagram for establishing a mixture model, detailing the runs and corresponding factor values (X_{11}-X_{13}) for each run.

Run	X_{11}	X_{12}	X_{13}
1	−1	−1	0
2	−1	1	0
3	1	−1	0
4	1	1	0
5	−1	0	−1
6	−1	0	1
7	1	0	−1
8	1	0	1
9	0	−1	−1
10	0	−1	1
11	0	1	−1
12	0	1	1
13	0	0	0
14	0	0	0
15	0	0	0

Appendix A. Particle density and PSD measurement

In this study, particle size was measured based on volume, following a two-step process. First, a set of pellet and sinter particles were scanned using X-ray computed tomography (CT). The volume of each particle (V_p) was extracted using Dragonfly, while the particle mass (m_p) was measured using a scale. The particle density was then calculated as

$$\rho_p = \frac{m_p}{V_p} \tag{A.1}$$

It is important to note that V_p represents the envelope volume, as internal pores were not accounted for in the scans. The density calculation was based on 15 particles for both pellets and sinter, and the average values are reported in Table 2.

Next, the particle mass distributions for pellets and sinter were obtained by sampling each material and measuring the individual particle masses. These mass distributions were then converted to volume

Table C.1
Simulation results for pellets based on the EDD from Table B.1, with each value representing the average of three replications per run.

Run	t_d	m_h	MSE	H_c	ϕ_h
1	4.0100	33.5197	0.0007	0.1251	0.4465
2	5.0967	55.7326	0.0043	0.2595	0.4714
3	4.0633	30.1511	0.0015	0.1145	0.4349
4	4.5267	40.5656	0.0001	0.1647	0.4417
5	3.6300	31.3809	0.0015	0.1071	0.4394
6	5.0167	48.3614	0.0016	0.2210	0.4778
7	3.9033	23.1746	0.0040	0.0809	0.4374
8	4.5400	39.2924	0.0001	0.1618	0.4415
9	4.6433	46.2929	0.0009	0.2068	0.4651
10	4.7400	47.9065	0.0013	0.2121	0.4664
11	4.4433	36.5325	0.0002	0.1495	0.4413
12	4.4267	38.7926	0.0001	0.1554	0.4395
13	3.4233	43.7052	0.0005	0.1878	0.4686
14	6.0500	50.1544	0.0019	0.2310	0.4636
15	3.2833	35.7038	0.0003	0.1451	0.4477
16	5.9567	38.1153	0.0002	0.1557	0.4340
17	3.6233	28.2102	0.0023	0.0973	0.4317
18	4.1533	34.1265	0.0005	0.1309	0.4471
19	3.6900	31.0224	0.0015	0.1031	0.4368
20	5.4267	56.1562	0.0047	0.2605	0.4669
21	3.6733	32.9340	0.0007	0.1303	0.4461
22	4.0633	33.8496	0.0007	0.1289	0.4415
23	4.8267	52.7997	0.0027	0.2368	0.4620
24	4.9933	55.0883	0.0036	0.2420	0.4605
25	2.6567	29.1183	0.0020	0.1020	0.4512
26	5.0167	35.7133	0.0003	0.1434	0.4388
27	3.7533	50.4197	0.0019	0.2276	0.4638
28	6.1633	56.5576	0.0041	0.2548	0.4564
29	3.5867	29.7003	0.0017	0.1060	0.4370
30	3.6400	30.7594	0.0015	0.1071	0.4358
31	4.7667	46.9119	0.0011	0.2132	0.4665
32	4.9767	48.8268	0.0014	0.2197	0.4643
33	2.3967	25.7171	0.0034	0.0807	0.4442
34	5.1067	33.6835	0.0007	0.1269	0.4303
35	3.5867	44.3179	0.0006	0.1994	0.4704
36	6.1633	50.7879	0.0020	0.2320	0.4594
37	3.1933	41.6968	0.0003	0.1776	0.4660
38	5.3000	47.4914	0.0011	0.2086	0.4540
39	3.3933	43.5355	0.0004	0.1908	0.4611
40	5.9533	50.2688	0.0016	0.2192	0.4536
41	4.6167	46.9960	0.0009	0.2061	0.4590
42	4.6433	47.6600	0.0010	0.2031	0.4592
43	4.6400	47.0915	0.0010	0.2028	0.4592
44	4.6500	46.5801	0.0008	0.2049	0.4595
45	4.6633	47.1445	0.0010	0.2080	0.4591

Table C.2
Simulation results for sinter based on the EDD from Table B.1, with each value representing the average of three replications per run.

Run	t_d	m_h	MSE	H_c	ϕ_h
1	4.5667	41.5630	0.00005	0.1999	0.4774
2	5.1533	46.2120	0.0011	0.2373	0.5038
3	4.5200	40.8297	0.00005	0.1871	0.4591
4	4.9600	46.7408	0.0007	0.2346	0.4857
5	3.8433	37.0293	0.0007	0.1521	0.4408
6	5.3833	42.4819	0.0004	0.2234	0.5116
7	3.8733	34.9315	0.0012	0.1446	0.4350
8	5.1133	44.5275	0.0004	0.2229	0.4824
9	4.8367	43.9556	0.0004	0.2240	0.4932
10	4.9200	44.2262	0.0004	0.2263	0.4955
11	4.7800	44.2366	0.0003	0.2140	0.4767
12	4.8300	44.2746	0.0003	0.2218	0.4791
13	3.5433	42.1239	0.0001	0.2100	0.4930
14	5.7433	46.0938	0.0007	0.2313	0.4895
15	3.4733	41.4836	0.0001	0.2017	0.4823
16	5.5667	45.5728	0.0005	0.2247	0.4705
17	3.5800	33.1600	0.0020	0.1300	0.4226
18	4.9633	40.4926	0.00005	0.1962	0.4834
19	3.9800	37.6691	0.0005	0.1619	0.4510
20	5.4933	45.2231	0.0010	0.2380	0.5068
21	4.4767	40.8147	0.00004	0.1908	0.4714
22	4.5667	41.3010	0.00003	0.1958	0.4730
23	4.9433	46.3014	0.0009	0.2355	0.4961
24	5.2167	46.2307	0.0009	0.2392	0.4945
25	3.2233	37.6316	0.0002	0.1805	0.4789
26	5.2767	42.0311	0.0001	0.2026	0.4676
27	3.6833	43.3834	0.0003	0.2182	0.4959
28	5.9500	47.9307	0.0013	0.2471	0.4910
29	3.7533	36.1631	0.0009	0.1509	0.4383
30	3.8900	36.5916	0.0009	0.1520	0.4403
31	5.1900	42.1991	0.0002	0.2174	0.4987
32	5.2800	43.1848	0.0004	0.2223	0.5039
33	2.6200	33.3795	0.0020	0.1147	0.4477
34	4.4733	37.5370	0.0006	0.1596	0.4394
35	3.7600	40.3493	0.0001	0.2063	0.5032
36	6.1533	44.0654	0.0005	0.2282	0.4951
37	3.4567	40.8429	0.0001	0.2041	0.4912
38	5.5467	44.8779	0.0005	0.2253	0.4811
39	3.5400	40.9562	0.0001	0.2015	0.4907
40	5.8267	46.3883	0.0007	0.2341	0.4820
41	4.8467	44.2215	0.0004	0.2221	0.4863
42	4.8700	44.5199	0.0004	0.2159	0.4892
43	4.8567	44.5925	0.0004	0.2236	0.4886
44	4.8600	44.6280	0.0003	0.2183	0.4853
45	4.8700	44.5479	0.0005	0.2231	0.4891

Table C.3
Simulation results for the pellet–sinter mixture based on the EDD from Table B2, with each value representing the average of three replications per run.

Run	t_d	m_h	MSE
1	4.5400	39.8087	0.00003
2	4.9333	44.4751	0.0004
3	4.5733	39.6012	0.0001
4	4.8933	43.8056	0.0003
5	4.0300	34.7813	0.0007
6	5.1433	42.9999	0.0003
7	4.0733	33.5387	0.0009
8	4.9400	43.2776	0.0003
9	3.8100	32.2339	0.0013
10	4.8500	40.8457	0.0001
11	4.1433	34.7597	0.0006
12	5.2433	45.3094	0.0006
13	4.8267	42.8658	0.0002
14	4.8133	42.7009	0.0002
15	4.7733	43.2286	0.0002

distributions using the corresponding values of ρ_p. Finally, the data were transformed into equivalent spherical diameter distributions, as shown in Fig. 12.

Appendix B. Experimental design diagrams

The EDD for the pellet simulations is shown in Table B.1. The EDD for the sinter simulations is identical, with X_1-X_5 being replaced by X_6-X_{10}, respectively. The EDD for the mixture simulations is shown in Table B.2.

Appendix C. DEM simulation results

See Tables C.1–C.3.

Data availability

Data will be made available on request.

References

[1] Raïsa Roeplal, Yusong Pang, Allert Adema, Jan van der Stel, Dingena Schott, Modelling of phenomena affecting blast furnace burden permeability using the discrete element method (DEM) – A review, Powder Technol. (ISSN: 0032-5910) 415 (2023) 118161, http://dx.doi.org/10.1016/j.powtec.2022.118161.

[2] Thomas Roessler, Christian Richter, André Katterfeld, Frank Will, Development of a standard calibration procedure for the DEM parameters of cohesionless bulk materials – part I: Solving the problem of ambiguous parameter combinations, Powder Technol. (ISSN: 0032-5910) 343 (2019) 803–812, http://dx.doi.org/10.1016/j.powtec.2018.11.034.

[3] Raïsa Roeplal, Yusong Pang, Dingena Schott, Effects of pellet-sinter interaction parameters on component segregation and bed porosity considering flow velocity and mixture composition: A DEM study, Adv. Powder Technol. (ISSN: 0921-8831) 35 (2) (2024) 104322, http://dx.doi.org/10.1016/j.apt.2023.104322.

[4] Chengzhi Li, Tom Honeyands, Damien O'Dea, Roberto Moreno-Atanasio, The angle of repose and size segregation of iron ore granules: DEM analysis and experimental investigation, Powder Technol. (ISSN: 0032-5910) 320 (2017) 257–272, http://dx.doi.org/10.1016/j.powtec.2017.07.045.

[5] Peiyong Qiu, Thomas Pabst, Waste rock segregation during disposal: Calibration and upscaling of discrete element simulations, Powder Technol. (ISSN: 0032-5910) 412 (2022) 117981, http://dx.doi.org/10.1016/j.powtec.2022.117981.

[6] Zilin Yan, Sam K. Wilkinson, Edmund H. Stitt, Michele Marigo, Investigating mixing and segregation using discrete element modelling (DEM) in the Freeman FT4 rheometer, Int. J. Pharm. (ISSN: 0378-5173) 513 (1–2) (2016) 38–48, http://dx.doi.org/10.1016/j.ijpharm.2016.08.065.

[7] Edouard Izard, Maxime Moreau, Pascal Ravier, Discrete element method simulation of segregation pattern in a sinter cooler charging chute system, Particuology (ISSN: 1674-2001) 59 (2021) 34–42, http://dx.doi.org/10.1016/j.partic.2020.08.004.

[8] Mohammadreza Alizadeh, Ali Hassanpour, Mehrdad Pasha, Mojtaba Ghadiri, Andrew Bayly, The effect of particle shape on predicted segregation in binary powder mixtures, Powder Technol. (ISSN: 0032-5910) 319 (2017) 313–322, http://dx.doi.org/10.1016/j.powtec.2017.06.059.

[9] Delft High Performance Computing Centre (DHPC), DelftBlue Supercomputer (Phase 2), 2024, https://www.tudelft.nl/dhpc/ark:/44463/DelftBluePhase2.

[10] Raymond D. Mindlin, Compliance of elastic bodies in contact, J. Appl. Mechanics-Trans. the Asme 16 (1949) 259–268, https://api.semanticscholar.org/CorpusID:111913131.

[11] Jun Ai, Jian-Fei Chen, J. Michael Rotter, Jin Y. Ooi, Assessment of rolling resistance models in discrete element simulations, Powder Technol. (ISSN: 0032-5910) 206 (3) (2011) 269–282, http://dx.doi.org/10.1016/j.powtec.2010.09.030.

[12] Han Wei, Hao Nie, Ying Li, Henrik Saxén, Zhijun He, Yaowei Yu, Measurement and simulation validation of DEM parameters of pellet, Sinter Coke Part. Powder Technol. (ISSN: 0032-5910) 364 (2020) 593–603, http://dx.doi.org/10.1016/j.powtec.2020.01.044.

[13] Arijit Chakrabarty, Rituparna Biswas, Saprativ Basu, Samik Nag, Characterisation of binary mixtures of pellets and sinter for DEM simulations, Adv. Powder Technol. (ISSN: 0921-8831) 33 (1) (2022) 103358, http://dx.doi.org/10.1016/j.apt.2021.11.010.

[14] Douglas C. Montgomery, Montgomery Design and Analysis of Experiments, nineth ed., John Wiley & Sons, Inc., ISBN: 9781119113478, 2022.

[15] D.R. Jensen, Efficiencies of some small second-order designs, Statist. Probab. Lett. (ISSN: 0167-7152) 21 (4) (1994) 255–261, http://dx.doi.org/10.1016/0167-7152(94)90135-X.

[16] G. Derringer, R. Suich, Simultaneous optimization of several response variables, J. Qual. Technol. 12 (4) (1980) 214–219, http://dx.doi.org/10.1080/00224065.1980.11980968.

[17] Luciana Vera Candioti, María M. De Zan, María S. Cámara, Héctor C. Goicoechea, Experimental design and multiple response optimization. Using the desirability function in analytical methods development, Talanta (ISSN: 0039-9140) 124 (2014) 123–138, http://dx.doi.org/10.1016/j.talanta.2014.01.034.

[18] X. Mu, W. Qi, Z. Zhang, G. Lv, S. Zhang, T. Wang, Parameter measurement and calibration in discrete element simulation of broken sweet potato seedlings, Am. J. Biochem. Biotechnol. 17 (2021) 256–266, http://dx.doi.org/10.3844/ajbbsp.2021.256.266.

[19] C. Hernández-Vielma, D. Estay, M. Cruchaga, Response surface methodology calibration for DEM study of the impact of a spherical bit on a rock, Simul. Model. Pr. Theory (ISSN: 1569-190X) 116 (2022) 102466, http://dx.doi.org/10.1016/j.simpat.2021.102466.

[20] W. Jiang, L. Wang, J. Tang, Y. Yin, H. Zhang, T. Jia, J. Qin, H. Wang, Q. Wei, Calibration and experimental validation of contact parameters in a discrete element model for tobacco strips, Processes 10 (2022) http://dx.doi.org/10.3390/pr10050998.

[21] G. Shi, J. Li, L. Ding, Z. Zhang, H. Ding, N. Li, Z. Kan, Calibration and tests for the discrete element simulation parameters of fallen jujube fruit, Agriculture 12 (2022) http://dx.doi.org/10.3390/agriculture12010038.

[22] Y. Yu, S. Ren, J. li, J. Chang, S. Yu, C. Sun, T. Chen, Calibration and testing of discrete element modeling parameters for fresh goji berries, Appl. Sci. 12 (2022) http://dx.doi.org/10.3390/app122211629.

[23] Jianzhong Zhu, Meng Zou, Yansong Liu, Kai Gao, Bo Su, Yingchun Qi, Measurement and calibration of DEM parameters of lunar soil simulant, Acta Astronaut. (ISSN: 0094-5765) 191 (2022) 169–177, http://dx.doi.org/10.1016/j.actaastro.2021.11009.

[24] X. Wang, W. Wu, H. Jia, Calibration of discrete element parameters for simulating wheat crushing, Nutrition 11 (2023) 7751–7764, http://dx.doi.org/10.1002/fsn3.3693.

[25] Biao Xie, Jinyin Bai, Jiagang Yan, Shibo Zhao, Nian Liu, Qiang Zhang, Calibration of white rice simulation parameters based on discrete element method, INMATEH Agric. Eng. 71 (2023) 215–224, http://dx.doi.org/10.35633/inmateh-71-18.

[26] Fahui Yuan, Hanwen Yu, Lin Wang, Yinyan Shi, Xiaochan Wang, Hui Liu, Parameter calibration and systematic test of a discrete element model (DEM) for compound fertilizer particles in a mechanized variable-rate application, Agronomy (ISSN: 2073-4395) 13 (3) (2023) http://dx.doi.org/10.3390/agronomy13030706.

[27] F. Zhang, R. Yangdao, Y. Wang, R. He, P. Li, Calibration of contact parameters of fresh-eating jujube based on discrete element method: Yuancui jujube in brittle ripe stage, Int. J. Food Prop. 27 (2024) 1–18, http://dx.doi.org/10.1080/10942912.2024.2379874.

[28] M. Fransen, M.D. Langelaar, Schott including stochastics in metamodel-based DEM model calibration, Powder Technol. 406 (2022) 117400, http://dx.doi.org/10.1016/j.powtec.2022.117400.

[29] G.B. McBride, A proposal for strength-of-agreement criteria for Lin's Concordance Correlation Coefficient, NIWA Client Report: HAM2005-062, https://www.medcalc.org/download/pdf/McBride2005.pdf.